metals

MDPI

Article

Experimental Study on the Thermal Stability of Aluminum Alloy 7075-T651 Structural Parts after Rolling Correction

Laixiao Lu [1], Meizhen Qin [1], Xiaodong Jia [2,*], Zhonglei Wang [1], Qingqiang Chen [1], Jie Sun [1] and Shourong Jiao [1]

[1] School of Mechanical and Electrical Engineering, Shandong Jianzhu University, No. 1000, Fengming Road, Licheng District, Jinan 250101, China
[2] School of Science, Shandong Jianzhu University, No. 1000, Fengming Road, Licheng District, Jinan 250101, China
* Correspondence: jxdfzh1996@sdjzu.edu.cn

Abstract: The rolling correction process can eliminate machining distortions of aluminum alloy 7075-T651 structural parts. The thermal stability of the corrected structural parts under the action of temperature loading, especially the macroscopic shape stability, is key to ensure the safe service of mechanical equipment. In this study, different thermal loads were used to postprocess aluminum alloy 7075-T651 structural parts after rolling correction. The thermal stability of the rolled samples was analyzed by characterizing the microstructure and physical and mechanical properties. The results show no obvious change compared to rolling in the distortion of the parts after temperature treatments at 120 °C, 160 °C, 230 °C and 300 °C; the distortion changes were only 10.48%, 2.74%, 8.13% and 8.70%, respectively. The residual stresses in the rolling areas of the samples decreased by 35.58%, 26.08%, 75.97% and 83.13%, respectively. The microhardness also showed a decreasing trend. There was no obvious change after treatment at 120 °C, but the hardness decreased by approximately 5%, 23% and 56%, respectively, after treatments at other temperatures. However, the rolling stress relaxed under thermal stress. The microstructure change analysis shows that the material microstructure is mainly dominated by static reversion at lower thermal loads. With increasing thermal load, the samples are mainly affected by the static recrystallization effect, the microstructure is gradually blurred, and the hardness decreases significantly. In conclusion, although the residual stresses introduced by rolling would occur in different degrees of stress relaxation under the thermal load, the microstructure changes caused by thermal load did not significantly affect the macroscopic distortion of the samples, and the macroscopic shape of the structural parts after rolling correction had good thermal stability.

Keywords: rolling correction; distortion stability; thermal load; residual stress; aluminum alloy 7075-T651

check for updates

Citation: Lu, L.; Qin, M.; Jia, X.; Wang, Z.; Chen, Q.; Sun, J.; Jiao, S. Experimental Study on the Thermal Stability of Aluminum Alloy 7075-T651 Structural Parts after Rolling Correction. *Metals* **2023**, *13*, 213. https://doi.org/10.3390/met13020213

Academic Editors: Tomoyoshi Maeno and Franc Zupanič

Received: 11 December 2022
Revised: 17 January 2023
Accepted: 18 January 2023
Published: 21 January 2023

Copyright: © 2023 by the authors. Licensee MDPI, Basel, Switzerland. This article is an open access article distributed under the terms and conditions of the Creative Commons Attribution (CC BY) license (https://creativecommons.org/licenses/by/4.0/).

1. Introduction

Thin-walled structural parts made of aluminum alloy 7075 are widely used in the automotive, marine, defense and aviation industry, such as frames, ribs and other mechanical parts, due to their excellent specific strength, specific stiffness and corrosion resistance [1–3]. During the computer numerical control (CNC) machining process of such thin-walled structural parts, a large amount of blank material is removed, and the material removal rate is as high as 98% [4]. Structural parts are affected by the coupling of blank stress, machining stress, cutting force, cutting heat, and other factors, which lead to the general problem of machining distortion of structural parts; the internal residual stress and microstructure are complicated [5,6].

As it is difficult to control many factors, current technology is still unable to effectively predict and control the machining distortion of structural parts [7]. Therefore, it is necessary to adopt a postprocessing correction process to ensure the manufacturing accuracy of

structural parts and to meet the assembly requirements of the mechanical equipment. Rolling correction is a process that corrects distortion by applying bilateral rollers at the tops of flanges, stiffeners and other structures of structural parts. Residual stress is a self-balancing internal stress that remains in the object after the external force is removed [8]. During the rolling process, the material in the rolled area undergoes severe plastic distortion, and high-amplitude residual compressive stress is introduced. The result is reverse distortion of the workpiece that offsets and corrects machining distortion [9].

The macroscopic distortion stability of structural parts is the key issue to ensure their service reliability. In the service process of some mechanical equipment, aluminum alloy structural parts are greatly affected by thermal load. While the rolling correction process reduces distortion and prevents structural parts from being out of tolerance, it also further increases the complexity of the internal states, such as plastic distortion, residual stress, and microstructure, of the parts. This makes the macroscopic distortion stability of the structural parts under thermal load unknown. Previous studies have shown that the evolution of the microstructure is the essential cause of irreversible deformation of materials [10]. In terms of microstructure, the evolution of the precipitation of the second phase and microstructural defects can lead to changes in the length of the material [11,12]. In the process of these microstructure changes, the microscopic yield strength and residual stress distribution characteristics of the material are also important indicators that affect the size change of the material [13]. Characteristics such as the elastic–plastic response of the grain can affect the microplastic deformation of the material [14]. High temperature causes significant changes in the hardness, ductility and other characteristics of aluminum alloys [15–17], reduces the microyield strength of the material, and affects the dimensional stability of the material. In addition, the stress state in the material more significantly determines the mechanical properties and fatigue life [18]. The high-amplitude residual stress introduced by the plastic distortion of aluminum alloys is easily affected by external loads such as temperature, and stress relaxation occurs [19,20]. Changes in residual stress may cause dimensional changes in structural parts [21]. If these changes in microstructure and material properties lead to changes in the macroscopic size and shape of the sample, the structural parts will be subjected to additional external forces in the assembly, which will deteriorate the service performance of the structural parts and affect their service life.

Therefore, it is of great significance to study the stability of aluminum alloy structural parts (after rolling correction) when they undergo thermal loading to ensure their safe use. In this paper, the influence of different thermal loads on the thermal stability of structural parts after rolling correction was studied by using structural parts of AA 7075-T651 as samples. To characterize the macroscopic characteristics and physical and mechanical properties of the rolling area and the milling area of the structural parts in different states, the macroscopic size distortion, residual stress and microhardness of the samples after milling, rolling correction and different thermal load treatments were investigated. The microstructure of each sample was analyzed by scanning electron microscopy (SEM), and the influence mechanism of different thermal loads on the thermal stability of the structural parts after rolling correction was analyzed.

2. Materials and Methods

2.1. Materials and Rolling Correction Process

The test material was an AA 7075-T651 plate with a thickness of 32 mm produced by Chinalco Southwest Aluminum Company, and its chemical composition is shown in Table 1. The test samples were aluminum alloy thin-walled T-shaped structural parts formed by integral milling, with a length of 150 mm, a width of 30 mm, and a flange thickness of 2.5 mm, as shown in Figure 1.

Table 1. AA 7075-T651 chemical composition.

Element	Zn	Mg	Cu	Fe	Si	Ti	Cr	Mn	Al
Wt (%)	5.7	2.4	1.5	0.35	0.32	0.11	0.2	0.16	Remainder

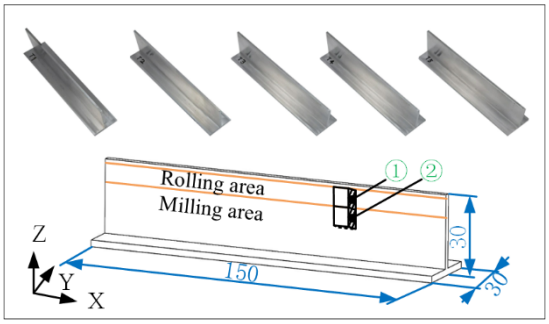


Figure 1. Samples used in the test.

Five samples of the same size were designed for the test, namely, T1, T2, T3, T4 and T5. Among them, the T1 sample was only processed by the rolling correction process, and the T2–T5 samples were first processed by the rolling correction process and then heat treated under different thermal loads. The rolling correction process was performed using a double-sided rolling correction device that was designed and made in this laboratory, as shown in Figure 2. The rolling area was the area on both sides of the top of each sample flange, the diameter of the roller was 28 mm, and the width of the roller was 8 mm. In actual production, the selection of rolling pressure and rolling passes needs to be determined according to the machining distortion of the workpiece to achieve the purpose of distortion correction. According to previous research and practical experience, the rolling force is generally in the range of 1500–5000 N, and the number of rolling passes is no more than 6. To better study the stability of the macroscopic distortion and physical and mechanical properties of the samples under thermal loading due to the rolling calibration process and to obtain obvious experimental phenomena, larger rolling process parameters were selected, that is, a rolling force of 4000 N and 6 rolling passes.

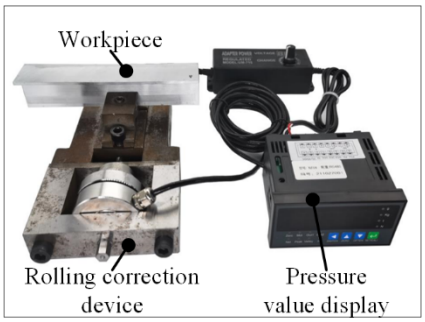


Figure 2. Rolling correction processing of structural parts.

2.2. Thermal Load Treatment

A KSL-1200X-J box-type heating furnace from Hefei Kejing Materials Co., Ltd., (Hefei, China) was used for heat treatment. In general, AA 7075 has high strength and especially good low-temperature strength below 150 °C [22]. In the heat treatment process, the double-step aging system of AA 7075-T651 is the main factor affecting the comprehensive properties of the plate, and aging temperatures of 120 °C and 160 °C are generally selected [23]. In industry, AA 7075 in the T6 state is often heated to 200–260 °C for between tens of seconds and minutes and then rapidly cooled to restore the plasticity of the alloy. When the material is at 300–350 °C, the recrystallization of the aluminum alloy reaches a higher degree. Based

on this, the heating scheme of the sample was selected. The heating scheme is shown in Table 2. The heating scheme of the furnace was controlled by a program. Each sample was heated to the target temperature at a heating rate of 10 °C/min in the furnace and then kept for 1 h. After cooling to 100 °C in the furnace, it was removed for air cooling.

Table 2. Thermal load treatment scheme.

Sample Number	Heating Rate	Maximum Temperature	Soaking Time
T1	Contrast sample		
T2	10 °C/min	120 °C	1 h
T3	10 °C/min	160 °C	1 h
T4	10 °C/min	230 °C	1 h
T5	10 °C/min	300 °C	1 h

2.3. Sample Test Process

The test procedure of the samples was carried out at room temperature. The test process is shown in Figure 3. Thin-walled structural parts are generally directly milled from prestretched plates, and more important surfaces are selected as positioning references during part design and processing. For the T-shaped sample used in this test, the base selected during the design and manufacturing process was the bottom surface of the sample. Surface measurement accuracy is directly affected by the sampling method and sample size [24]. Therefore, the bottom surface of the sample was selected as the benchmark for distortion measurement, and the macroscopic distortion of the sample was characterized by the measured spatial position relationship of a large number of bottom feature points. The dimensional distortion of each sample after milling, rolling correction and thermal load treatment was measured by a Performance7107 coordinate measuring machine (CMM). The height data of the sample were measured intensively along the midline and both edges of the length direction at the bottom of the sample by using point measurement, and these data were fitted to the surface data for analysis. The size measurement points are shown in Figure 3d. The X-ray stress measurement method can measure the surface residual stress of the material without destroying the material and belongs to the field of nondestructive testing. The basic idea is that the lattice strain and macroscopic strain of the material caused by a certain stress state are consistent. The lattice strain (diffraction crystal plane spacing) is obtained by the X-ray diffraction technique, the macroscopic strain is obtained, and then the macroscopic stress is obtained by elastic mechanics. Therefore, according to the EN15305-2008, ASTME915-10, and GB/T7704-2017 standards for measuring residual stress by the X-ray stress measurement method [25], the residual stress of the surface layer of the sample was measured by a Proto-iXRD X-ray stress analyzer. The measurement method was the modified roll fixed Ψ method, the target was Cr-Kα, the diffraction index of the diffraction surface was (311), the diffraction angle was 139.5°, the exposure time was 5 s, and the Ψ angle was 0°, ±25°, ±35°, ±45° [26]. The residual stress measurement points of residual stress on the surface of the sample are shown in Figure 3e. There were four residual stress measurement points: measurement points #1, #2, and #3 were located in the rolling area to characterize the residual stress in the rolling area, and measurement point #4 was located in the milling area to characterize the residual stress in the milling area.

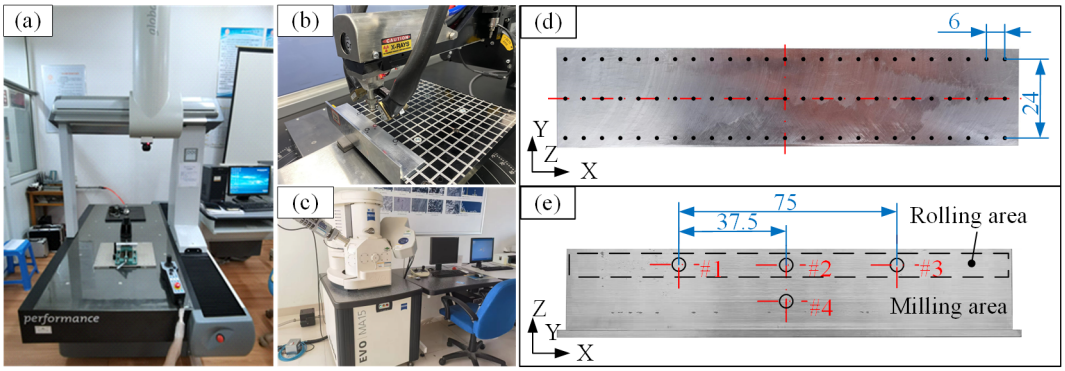


Figure 3. Measurement process of structural parts: (**a**) CMM tests, (**b**) residual stress detection, (**c**) SEM system, (**d**) CMM measurement point, and (**e**) residual stress measurement point.

The cutting position of the sample used to observe the microstructure is shown in Figure 1. Two samples for microstructure analysis, ① and ②, were cut from each test sample by electrical discharge machining (EDM). The normal direction of the sections of samples ① and ② was parallel to the rolling direction. Sample ① was located in the rolling area, and sample ② was located in the milling area. Samples ① and ② were ground using water and sandpaper, polished with flannel, and inlaid; the microhardness was measured, and they were then used for scanning electron microscope (SEM) observations after corrosion treatment.

The microhardness distribution of each sample was measured along the depth direction of the milling area and rolling area by a Huayuzhongxin HV-1000A microhardness tester. The applied load was 10 g, and the holding time was 5 s [27]. To improve the accuracy of the test results, the test was repeated three times at the same depth, and the average value was taken. The surface morphology of the milling area and the rolling area of the sample was characterized by a Zeiss-Smartzoom5 ultradeep field microscope. The microstructure morphology of the rolling area and milling area of each sample was analyzed by a Nikon-MA100 N metallographic microscope and Zeiss-EVO-MA15 SEM.

3. Results

3.1. Part Distortion

To obtain large plastic distortion and residual stresses for the observation and analysis of the test, the rolling parameters were set to the upper limit, which led to the distortion of the samples in the opposite direction. The macroscopic distortion of the bottom surface of the sample after the milling process, after the rolling correction and after the thermal load treatment is shown in Figure 4. After milling, the samples were relatively straight overall, and there was a slight processing distortion. The maximum distortion of the midline of the T2, T3, T4, and T5 samples was 0.007 mm, 0.004 mm, 0.013 mm and 0.008 mm, respectively. After the rolling correction process, the macroscopic shape of the samples changed to produce a bending distortion with the middle raised upward, and the maximum distortion of the midline of the sample reached 0.105 mm, 0.073 mm, 0.123 mm and 0.092 mm.

Figure 4 shows that the distortion diagrams of each sample after thermal load treatment and after rolling correction basically overlapped, and there was no obvious macroscopic dimensional distortion. The maximum distortions of the midline of the T2, T3, T4 and T5 samples were 0.094 mm, 0.071 mm, 0.113 mm and 0.084 mm, respectively. Compared with those after rolling correction, the distortion of the samples after thermal load treatment were 0.011 mm, 0.002 mm, 0.010 mm and 0.008 mm, respectively, and the distortion was only 10.48%, 2.74%, 8.13% and 8.70% of the size after rolling correction. The size of each sample did not change significantly after different thermal loading treatments, which indicated that the macroscopic size of each sample was very stable under the action of thermal loading.

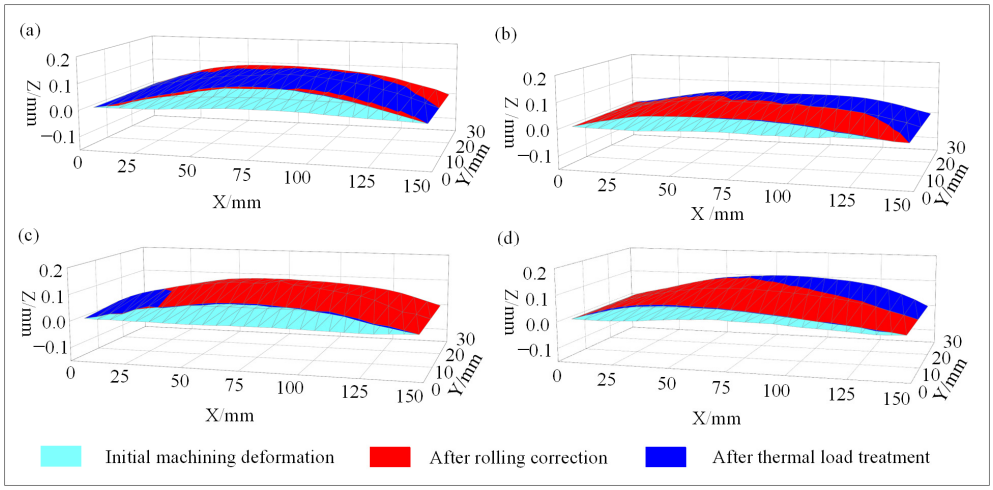


Figure 4. Macroscopic distortion diagrams of structural parts after milling, rolling correction and thermal load heat treatment: (**a**) T2/120 °C, (**b**) T3/160 °C, (**c**) T4/230 °C, and (**d**) T5/300 °C.

3.2. Residual Stress

The residual stress on the surface of the milling area (#4 measurement point) after rolling correction is shown in Figure 5. The residual stress in the milling area of each sample is shown as the residual compressive stress state. After milling, the surface layer of the sample generally had compressive stress with different amplitudes under the action of the cutting force. After different thermal loads, the residual stress in the milling area changed greatly. Compared with that after rolling correction, the residual compressive stress of the T3, T4 and T5 samples treated with different thermal loads decreased by 39.58 MPa, 8.82 MPa and 53.99 MPa, respectively, and the reduction rates were 55.42%, 14.34%, and 89.40%, respectively. In addition, the residual stress of the T2 sample after thermal load treatment increased by 15.03 MPa, and the residual stress change of the sample showed a large error band with poor reliability.

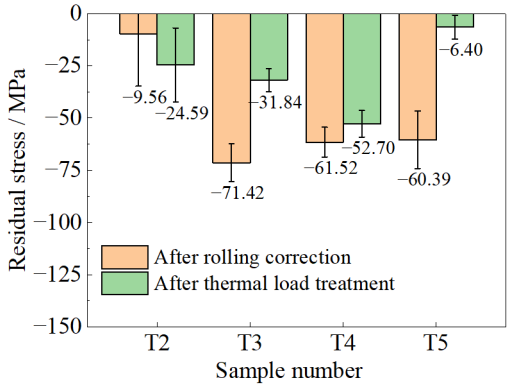


Figure 5. Residual stress detection results of the milling area after rolling correction and thermal load treatment.

The residual stress in the surface layer of the sample rolling area is shown in Figure 6. After rolling correction, the residual stress in the rolling area of each sample was in a residual compressive stress state. After different thermal load treatments, the residual stress of each sample was greatly reduced. After the T2, T3, T4, and T5 samples were subjected to thermal load treatment at 120 °C, 160 °C, 230 °C, and 300 °C, respectively, the residual compressive stress of the T2 and T3 samples decreased to a similar degree and that of the T4 and T5 samples decreased to a similar degree; the residual stresses of the T4 and T5 samples were reduced to a greater extent than those of the T2 and T3 samples. The residual

compressive stress of the T2 and T3 samples decreased by 35.58% and 26.08%, respectively, and that of the T4 and T5 samples decreased by 75.97% and 83.13%, respectively.

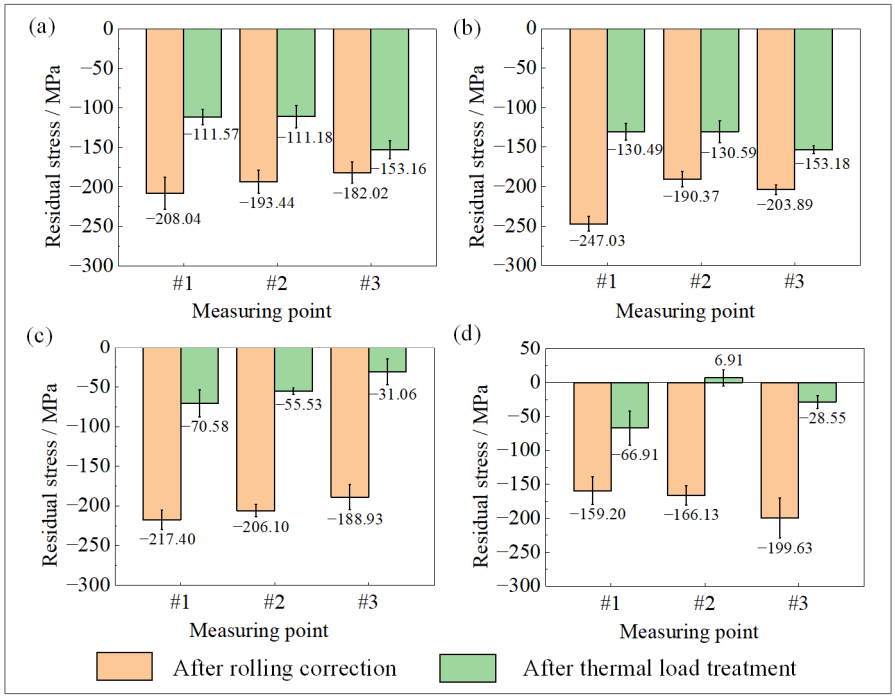


Figure 6. Residual stress test results of the rolling area after rolling correction and thermal load treatment: (**a**) T2/120 °C, (**b**) T3/160 °C, (**c**) T4/230 °C, and (**d**) T5/300 °C.

The residual stresses of the T2 and T3 samples are shown in Figure 6a,b, and their maximum residual stresses were reduced by 96.47 MPa and 116.54 MPa after thermal loading at 120 °C and 160 °C, respectively. With increasing thermal load, the residual stresses of the T4 and T5 samples are shown in Figure 6c,d, and their maximum reductions were 157.87 MPa and 171.08 MPa after treatment at 230 °C and 300 °C, respectively. In addition, the data measured at point #2 of the T5 sample after thermal load treatment showed positive values. The residual stress at this point has approached the stress-free state. Due to the influence of factors such as the surface texture of the material, the measurement results show positive values and error bands involving positive and negative ranges.

3.3. Microhardness

With the increase in the degree of plastic deformation during rolling, the surface layer of the rolling area exhibited work hardening. The strength and hardness of the surface layer (hardened layer) material were increased. The microhardness distribution along the depth direction of the shallow surface area of the T1 sample after the rolling correction treatment is shown in Figure 7. Within the depth range of the hardened layer, there was little difference between the microhardness values in the milling area and the rolling area, but the hardness of the rolling area was always greater than that of the milling area. The microhardness of the surface of the milling area was 170.1 $HV_{0.01}$, which gradually decreased to a matrix hardness value of 164.1 $HV_{0.01}$ with increasing depth, while the microhardness of the surface of the rolling area was 175.7 $HV_{0.01}$, which reached the matrix hardness at approximately 120 μm below the surface.

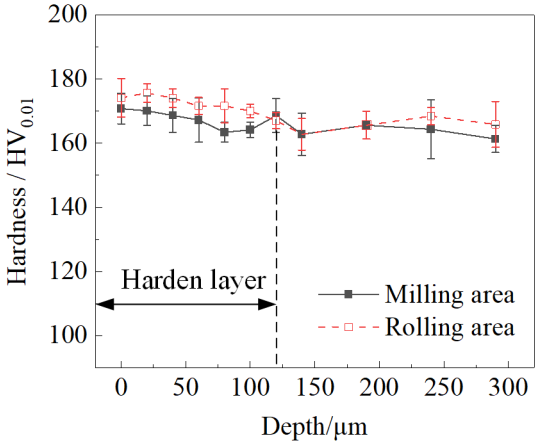


Figure 7. Microhardness distribution of the T1 sample along the depth direction after rolling correction treatment.

The microhardness distribution of the milling area and the rolling area of each sample after temperature treatment is shown in Figure 8. The microhardness trend of each sample in the depth range of the hardened layer was similar to that of Figure 7, which showed that the hardness of the rolling area was always greater than that of the milling area. Compared to the T1 sample treated only by rolling correction, the T2 sample treated by thermal loading at 120 °C did not show a significant change in hardness. However, with increasing thermal load, the microhardness of the milling area and the rolling area showed an obvious decreasing trend. Compared to the T1 sample, the hardness of the T3 sample was reduced by approximately 5%, that of the T4 sample was reduced by approximately 23%, and that of the T5 sample was reduced by approximately 56%, which adversely affected the material properties.

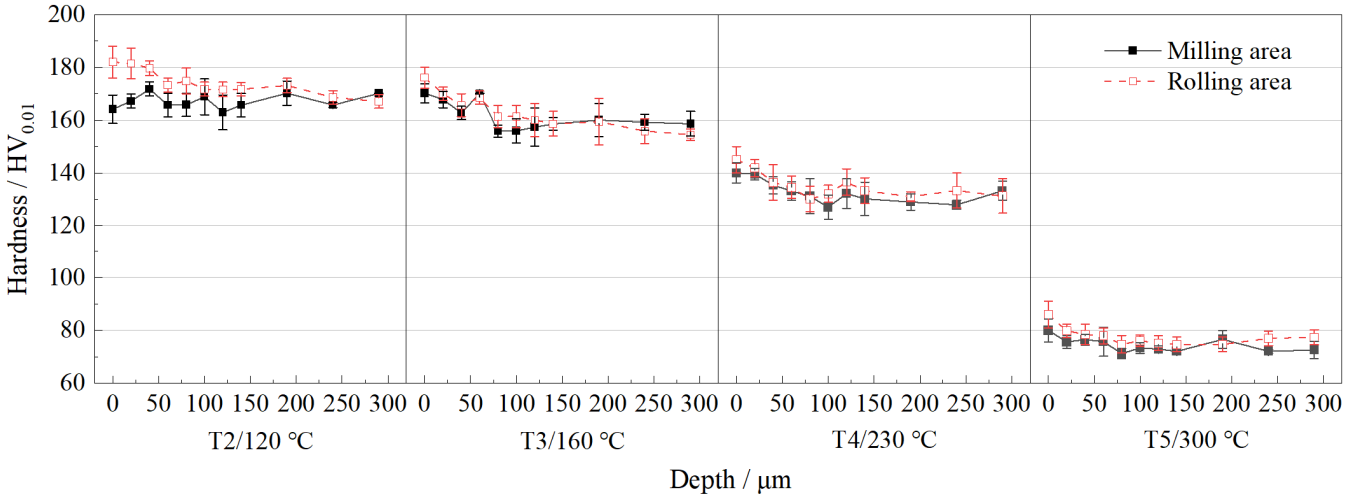


Figure 8. Microhardness distribution along the depth direction after different thermal loads.

3.4. Microstructure

The surface morphology and microstructure changes of the T1 sample after rolling correction treatment are shown in Figure 9. Significant microscopic plastic deformation occurred in the rolling area of the sample. There were a large number of milling marks composed of convex peaks and valleys on the surface of the milling area of the sample, as shown in Figure 9a,d. After the rolling correction treatment, the original valleys in the rolling area are filled with the surrounding convex peaks after deformation, and the surface morphology is smoother, as shown in Figure 9c,e. The surface topography change

in Figure 9 also shows that the plastic deformation phenomenon in the rolling area is affected by the quality of the material surface milling process. The rougher the material surface is, the more obvious the plastic deformation phenomenon.

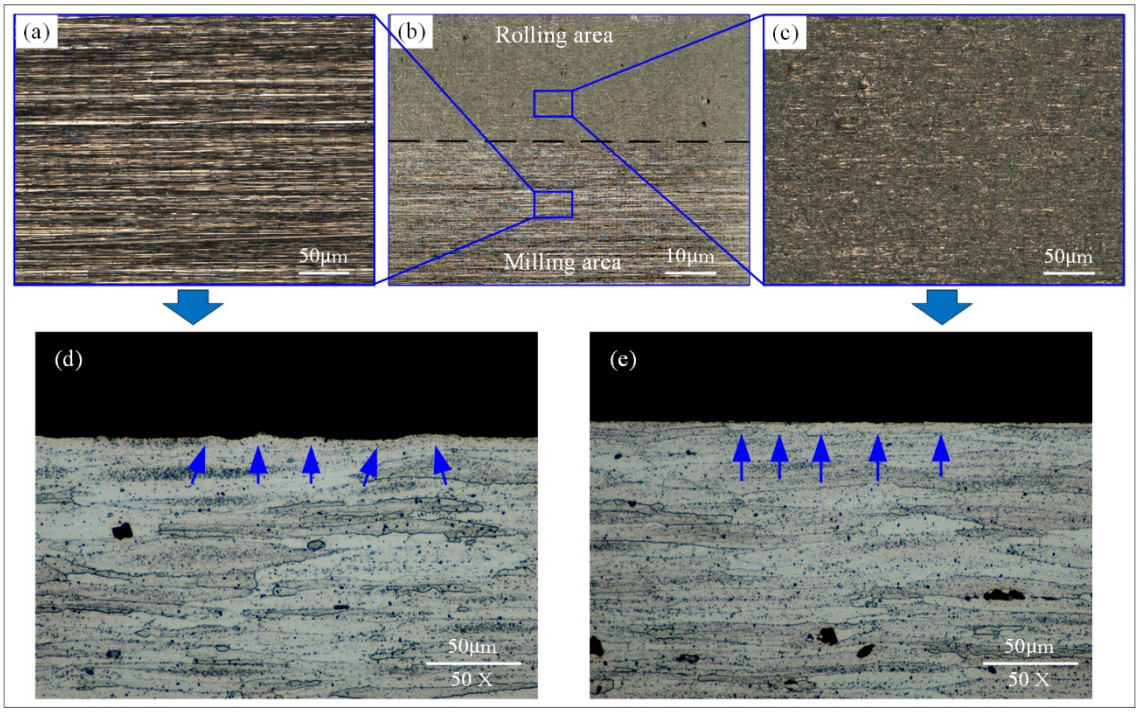


Figure 9. Changes in surface morphology and microstructure of T1 sample after rolling correction treatment: (**a**–**c**) surface morphology of rolling area and milling area; (**d**) microstructure of milling area in depth direction; and (**e**) microstructure of rolling area in depth direction.

The microstructure of the T1 sample after rolling correction is shown in Figure 10. The aluminum alloy exhibited an obvious fibrous deformation structure, and the grains were flattened and elongated along the width direction of the sheet. Some grains were affected by rolling distortion, which resulted in incomplete grain boundaries. After polishing and corrosion treatment, the regions of adjacent grains without grain boundaries were connected, and the SEM morphology showed a regional distribution of long grains. The T651 treatment of the aluminum alloy had a peak aging state. Dispersed phases distributed along grain boundaries and matrix precipitates distributed in regional clusters were observed on the surface of the sample. The generally accepted precipitation sequence for Al–Zn–Mg–Cu alloys is as follows: supersaturated solid solution (SSS) → GP zones → metastable η′ phase→ stable η phase [28]. The distribution of the GP zone is mainly related to the natural aging clusters formed by the aggregation of solute atoms in the aluminum matrix. Its volume is small and cannot be observed in Figures 10 and 11. The η phase is mainly precipitated along the grain boundary [29]. Some studies have shown that the GPI zone formed during aging below 100 °C will be dissolved during aging above 120 °C, and the GPII zone will be formed and further converted into η′ to produce a strengthening effect [30]. In addition to the GP zone and coarse η equilibrium phase, the dispersed η′ phase is the main precipitate. With increasing holding time, the precipitated phase in the alloy coarsens. Intergranular precipitates are coarser than intragranular precipitates and become discontinuously distributed during aging [31]. Therefore, it can be confirmed that the matrix precipitated phase in Figures 10 and 11 is mainly composed of a coarse η′ phase, and the precipitated phase distributed along the grain boundary is mainly composed of a coarse η phase [23].

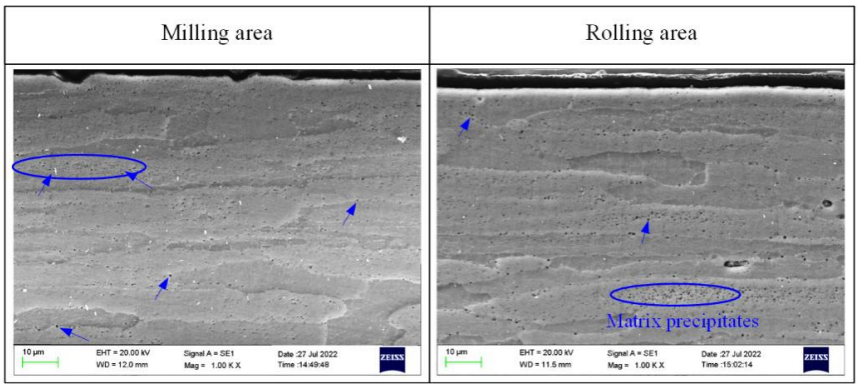


Figure 10. SEM morphology of the milling area and rolling area of the T1 sample after rolling correction only.

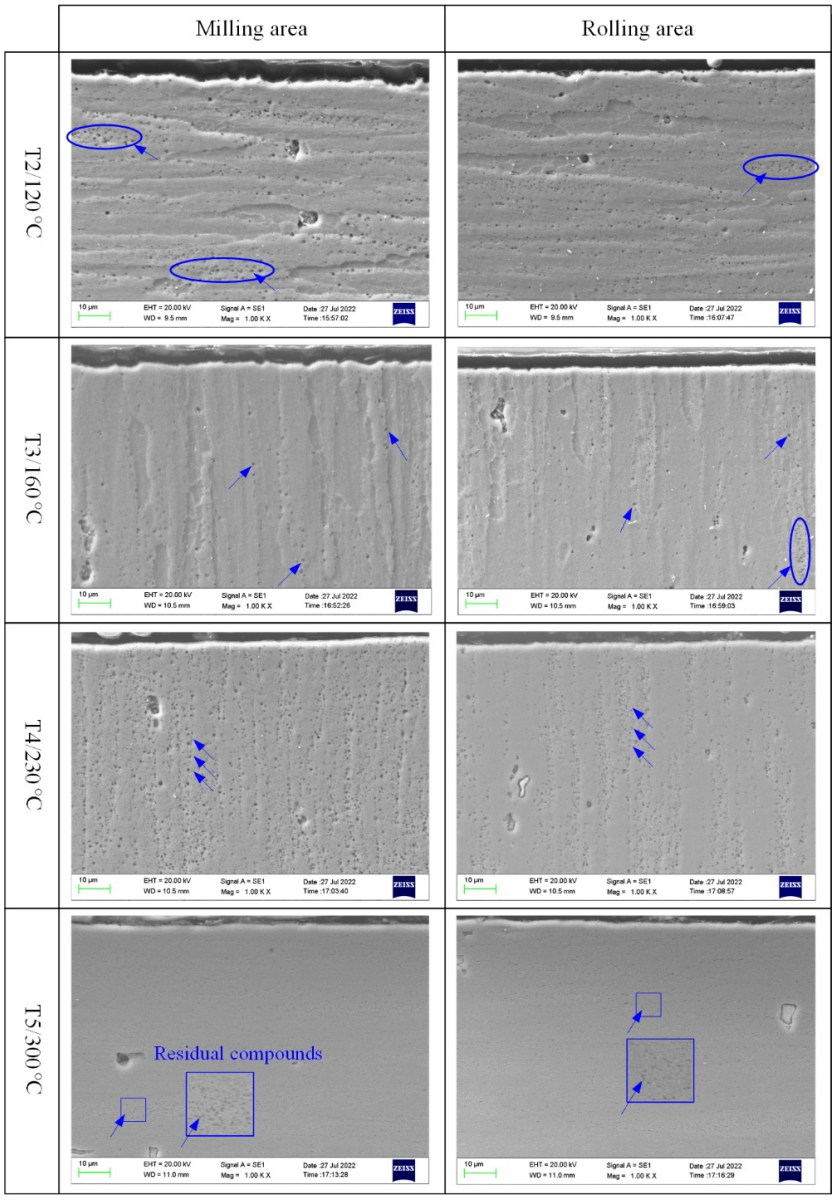


Figure 11. SEM morphology of the milling area and rolling area after different thermal load treatments.

The microstructure of the T2 sample after 120 °C thermal load treatment is shown in Figure 11. Compared with the sample treated only by rolling correction, there was no obvious change in the grain morphology of the milling area and the rolling area, and there were still obvious matrix precipitates on the metal surface. After the T3 sample was treated with a thermal load of 160 °C, the matrix precipitates of the cluster distribution had disappeared, the grain boundaries were still visible in the milling area along the width of the plate, and the grain boundaries were more incomplete in the rolling area due to the rolling effect. After heat treatment at 230 °C, the microstructure of the T4 sample had gradually blurred, and there were many coarse precipitates dispersed in the original grain boundary in the milling area, while there were fewer precipitates in the rolling area. After the T5 sample was treated at 300 °C, the microstructure was completely blurred, the grain boundaries and precipitated phases were no longer visible, and only some undissolved compounds remained in the matrix.

4. Discussion

According to the internal stress model proposed by Macherauch [32], the internal stress can be divided into three categories. Category I internal stress is the macroscopic stress suitable for the distortion volume. Category II internal stress is the stress between the crystal fragments after distortion. Category III internal stress is the stress caused by crystal distortion. Among them, category I internal stress is called macroscopic stress, and category II internal stress and category III internal stress are collectively called microscopic stress. Figure 9 shows that after the rolling correction treatment, under the action of "cutting peaks and filling valleys", the original valleys on the milling surface were filled with surrounding convex peaks, and the rolling surface underwent serious plastic deformation, resulting in the generation of microscopic stresses. At the same time, the core material in the rolling area was passively elastically deformed under the action of plastic deformation and elongation of the surface material, accompanied by macroscopic stress. For the whole sample, due to the effect of rolling, overall distortion of the middle upward bulge occurs, and macroscopic stress is generated throughout the whole sample. The distribution of the rolling area stress and macroscopic distortion compatible stress is shown in Figure 12. In the depth direction of the rolling area, there was a high-amplitude compressive stress on the surface of the material and a large tensile stress inside. In the overall structure, the upper part after rolling treatment manifested as compressive stress, and the lower half represented the tensile stress state.

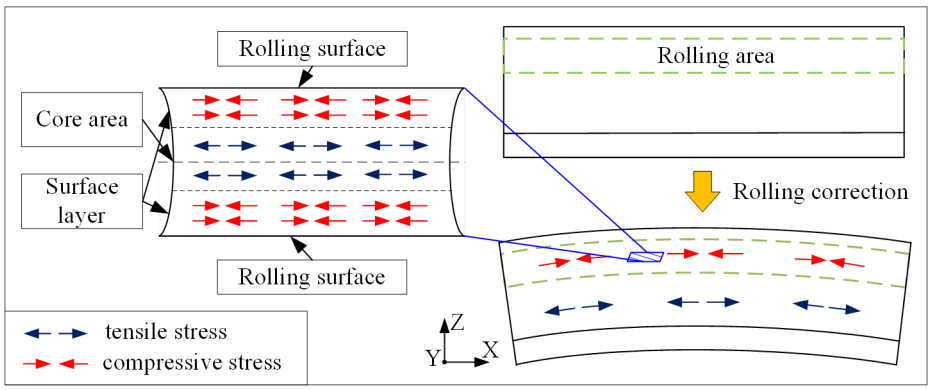


Figure 12. Rolling area and overall macroscopic stress distribution of samples after rolling correction.

According to the X-ray residual stress test method, the residual stress obtained by the test was mainly macroscopic stress, that is, category I internal stress. As shown in Figures 5 and 6, the residual stresses were reduced to different degrees after the thermal load treatment process, and the residual stresses were reduced to a greater extent as the treatment temperature increased. The change in the macroscopic shape of the sample is mainly affected by mechanical reasons and microstructural changes. The former changes

due to the stress generated or the relaxation of residual stress, and the latter is due to recrystallization and transformation of microscopic components [33]. Changes in both cases can eventually be expressed as changes in residual stress. The first case is manifested by rapid temperature rise, which generates a large temperature gradient inside the material and introduces new residual stresses under the effect of thermal expansion and contraction, causing the material to passively deform plastically due to residual stresses exceeding the microyield strength or incompatible internal strains [34,35]. The second case is manifested in the warming and holding process, and the dynamic changes in the internal organization of the material under the effect of thermal load cause volume changes, which in turn affect the internal stress balance, resulting in the redistribution of stress.

During the heating process of the thermal load treatment test, the temperature difference between the outer layer and the inner part of the thin-walled aluminum alloy sample was very small, the material yield strength in the T651 state was very high, and it was difficult to generate local plastic deformation during the heating process. Therefore, the residual stress reduction effect observed in Figures 5 and 6 was mainly achieved during the holding process. The elastic deformation energy and residual stress in the material were consumed and released through changes in the material structure, which in turn caused changes in local plastic deformation due to the evolution of the material organization, affecting the macroscopic shape of the sample.

In the process of thermal load treatment, the release process of energy storage of different cold distortion materials was also different. The release of metal energy storage is greatly affected by temperature. The release of alloy metal energy storage requires a higher temperature, and the release rate is lower than that of pure metal [22]. In general, during heat treatment, the release of energy storage in alloy materials was mainly achieved through static recovery and recrystallization [36].

Under a thermal load of 120 °C or 160 °C, as shown in Figure 11, the grain morphology of the sample did not change significantly. Due to the relatively low temperature, it was not enough to provide enough driving force to make the subcrystals merge to form recrystallized grains. During this thermal load treatment, the material was mainly static recovery. During the recovery process, the cellular structures formed by the division of the dislocation structure merge through the cross slip of the screw dislocation and the climbing of the edge dislocation to form a polygonization effect, which consumes a certain amount of strain energy. Since aluminum is a metal with high-level dislocation energy, the changes in dislocation aggregation, distribution state and vacancy diffusion are strong during the heating recovery process, which can reduce the category I internal stress while basically maintaining the process hardening and have a certain reduction effect on the category II and III internal stresses. In addition to the elastic deformation energy storage introduced by the rolling correction treatment, there is also residual thermal stress in the sample due to the uneven distribution of elastic energy, lattice defects (vacancies and dislocations) and temperature stored in the aluminum alloy matrix during manufacturing [37,38]. Under thermal loading at 120 °C and 160 °C, the elastic strain caused by these thermal and rolling residual stresses was recovered and relaxed by the reduction of stored energy and the elimination of defects [39].

In this recovery process, the grain morphology did not change significantly, and the change in the precipitation strengthening phase played a major role in the plastic deformation of the sample. The increase in temperature promotes the nucleation, growth and coarsening of the η phase. The aluminum alloy in the T651 state is already in the peak aging state, and its precipitated phases are mainly the GP zone and η′ phase. Therefore, the precipitated phase in the alloy gradually grows from the GP zone and η′ phase to form the η phase during the thermal load treatment of the aluminum alloy. The effect of the η′ phase on the strength is much greater than that of the η phase. With increasing temperature, the transformation of the η′ phase leads to a decrease in alloy strength [40]. However, as the main strengthening phase of AA 7075-T651, the η′ phase and η phase both play an effective role in pinning dislocations. Under the influence of strengthening, the microyield strength

of the sample is high, and dimensional deformation is difficult to occur [38]. However, in the rolling area, the original high-amplitude residual stress and deformation energy storage of the rolling surface would reduce the microyield strength of this area, and local plastic deformation might occur with the release of stress under the action of thermal load. As shown in Figure 9, the plastic deformation layer in the rolling area of the sample was very small. The deformation layer in the form of a concave valley filled with convex peaks would have contact gaps, which could adapt to the small plastic deformation and then only had an extremely small effect on the macroscopic shape of the sample. The original elastic strain in the core of the rolling area gradually relaxed with decreasing residual stress and gradually solidified into plastic strain under the obstruction of the surface plastic deformation layer. As shown in Figure 4, the samples after thermal loading at 120 °C or 160 °C had only local small size changes. The local plastic deformation produced during the recovery process did not have a noticeable effect on the macroscopic shape.

Recovery and recrystallization were in a competitive relationship. Once recrystallization began, the deformation substructure disappeared, and recovery was no longer carried out [22]. With increasing thermal load, in addition to recrystallization, the decomposition of the α(Al) solid solution and the aggregation of residual soluble compounds also occur. Since the decomposition products are densely distributed on the α(Al) matrix, the recrystallized grains become difficult to separate and observe. As shown in Figure 11, the changes in the microstructure and the decrease in microhardness after the 230 °C thermal load treatment indicated that the sample had undergone recrystallization, while the sample after the 300 °C thermal load treatment already had a higher level of recrystallization. Therefore, with increasing thermal load, the samples gradually changed from static recovery to static recrystallization control during the thermal load treatment at 230 °C and 300 °C.

As shown in Figure 11, the dispersed precipitates on the surface of the material were coarsened after the thermal load treatment at 230 °C. The grain boundary lost the strong pinning effect of strengthening precipitates. The change in the material matrix and the change in recrystallized grain size played an important role in the plastic deformation of the sample and became the key factors affecting the macroscopic shape of the sample. In this process, certain substructures became nucleation sites for recrystallized grain growth through particle-excited nucleation, and the elastic strain energy stored in the form of dislocations acted as a driving force to promote the growth and aggregation of recrystallized grains, which resulted in a more substantial reduction in residual stress and elastic strain. As the degree of recrystallization increases, the changes in grain orientation and texture ratio cause changes in the microscopic plastic strain of the aluminum alloy [10]. However, as shown in Figure 4, the macroscopic size of the sample after thermal load treatment at 230 °C and 300 °C had only local small size changes, and this localized small plastic deformation did not cause obvious macroscopic distortion of the sample.

Compared to the reversion process, the recrystallization process could fully eliminate the category I internal stress while also substantially eliminating the category II and III internal stresses and can even achieve the complete elimination of internal stress [22]. Compared with the samples treated at 120 °C and 160 °C, the residual stress of the samples treated at 230 °C and 300 °C was reduced to a greater extent, and the elastic strain energy of the samples was further reduced to a more balanced and stable state. The small local deformation caused by the change in the microstructure during heat treatment did not have a significant impact on the macroscopic distortion of the sample. However, the coarsening and dissolution of the reinforced precipitation phase caused a significant decrease in microhardness [41,42]. The rapid decrease in the microhardness of the sample after the thermal load treatment at 230 °C indicated that the material exhibited a softening effect [43]. The formation of low-dislocation recrystallized grains further improved the softening effect of the metal [44]. With the continuous improvement of the softening effect, the microhardness of the material was greatly reduced, and the microyield strength of the sample adversely affected the strength performance of the structural parts.

5. Conclusions

Stability tests were conducted for AA 7075-T651 structural parts after rolling correction and different thermal load treatments. The effects of different thermal loads on the macroscopic size distortion, residual stress, microhardness and microstructure of structural parts were analyzed. The influence mechanism of different thermal loads on the quality stability of structural parts was revealed.

(1) Compared to after rolling correction, the distortions of the samples were 0.011 mm, 0.002 mm, 0.010 mm and 0.008 mm after 120 °C, 160 °C, 230 °C and 300 °C thermal load treatments, respectively, and the changes were only 10.48%. 2.74%, 8.13%, and 8.70%, which indicated that the macroscopic dimensions of the rolling-corrected structural parts had good thermal stability under different thermal loads.

(2) Compared to after rolling correction, the residual stresses in the rolling area of the samples gradually decreased with increasing thermal load, and the average residual compressive stresses decreased by 35.58%, 26.08%, 75.97%, and 83.13% after 120 °C, 160 °C, 230 °C, and 300 °C treatments, respectively; the microhardness also showed a decreasing trend, with no significant change in hardness after treatment at 120 °C, but the hardness values of samples treated at 160 °C, 230 °C and 300 °C decreased by approximately 5%, 23% and 56%, respectively.

(3) The precipitates appeared in a process of growth, transformation, and resolvate with increasing thermal load. There were many matrix precipitates in the sample after 120 °C treatment. After 160 °C treatment, the matrix precipitates distributed in clusters gradually dissolved and disappeared. After 230 °C treatment, many coarse precipitates were dispersed at the original grain boundary position. After 300 °C treatment, only some undissolved compounds remained in the matrix.

(4) Under low thermal loads of 120 °C and 160 °C, the reduction in residual stress was mainly caused by static recovery. With increasing processing temperature, the reduction in residual stress was mainly affected by static recrystallization. Due to the combined influence of changes in precipitates, dislocation density, grain size, etc., the small local deformation caused by thermal load treatment did not have a significant impact on the macroscopic distortion of the sample.

Author Contributions: Funding acquisition, review and editing, experimental arrangement: L.L.; experimental arrangement, writing, data curation: M.Q.; CMM tests and revised: X.J.; residual stresses tests and revised: Z.W.; SEM observed and revised: Q.C.; microhardness tests and revised: J.S.; review and editing, supervision: S.J. All authors have read and agreed to the published version of the manuscript.

Funding: This research was funded by the National Natural Science Foundation of China (No. 51905313), Provincial Natural Science Foundation of Shandong (No. ZR2019BEE033) and Doctoral Research Foundation of Shandong Jianzhu University (XNBS1801).

Data Availability Statement: Not applicable.

Acknowledgments: In this section, The authors wish to acknowledge Xiangyu Wang of Jinan University for his help in the detection of residual stress, and Xue Song of Shandong special equipment inspection institute group Co., Ltd. for providing technical support for SEM.

Conflicts of Interest: The authors declare no conflict of interest.

References

1. Zhang, R.X.; Chiang, R.; Ren, Z.C.; Zhang, H.; Zhao, W.D.; Wang, G.X.; Vasudevan, V.K.; Dong, Y.L.; Ye, C. Fatigue Performance Improvement of 7075-T651 Aluminum Alloy by Ultrasonic Nanocrystal Surface Modification. *J. Mater. Eng. Perform.* **2022**, *31*, 2354–2363. [CrossRef]
2. Liu, W.M.; He, W.H.; Liu, L.; Li, J.; Pan, H.J.; Zhang, W.; Wang, Z.J. Microstructure and Tribological Properties of 7075-T651 Aluminum Alloy Affected by N-Ion Implantation. *J. Mater. Eng. Perform.* **2022**, *2022*, 1–9. [CrossRef]
3. ZawadaMichałowska, M.; Pieśko, P.; Józwik, J.; Legutko, S.; Kukiełka, L. A Comparison of the Geometrical Accuracy of Thin-Walled Elements Made of Different Aluminum Alloys. *Materials* **2021**, *14*, 7242. [CrossRef]

4. Denkena, B.; Boehnke, D.; de León, L. Machining induced residual stress in structural aluminum parts. *Prod. Eng.* **2008**, *2*, 247–253. [CrossRef]
5. Llanos, I.; Aurrekoetxea, M.; Agirre, A.; Lacalle, L.N.L.D.; Zelaieta, O. On-machine Characterization of Bulk Residual Stresses on Machining Blanks. *Procedia CIRP* **2019**, *82*, 406–410. [CrossRef]
6. Weng, Z.J.; Liu, X.Z.; Gu, K.X.; Guo, J.; Cui, C.; Wang, J.J. Modification of residual stress and microstructure in aluminium alloy by cryogenic treatment. *Mater. Sci. Technol.* **2020**, *36*, 1547–1555. [CrossRef]
7. Li, J.G.; Wang, S.Q. Distortion caused by residual stresses in machining aeronautical aluminum alloy parts: Recent advances. *Int. J. Adv. Manuf. Technol.* **2017**, *89*, 997–1012. [CrossRef]
8. Zhang, Y.; Wang, W.H.; Greer, A.L. Making metallic glasses plastic by control of residual stress. *Nat. Mater.* **2006**, *5*, 857–860. [CrossRef]
9. Lu, L.X.; Sun, J.; Han, X.; Xiong, Q.C. Study on the Surface Integrity of a Thin-Walled Aluminum Alloy Structure after a Bilateral Slid Rolling Process. *Metals* **2016**, *6*, 99. [CrossRef]
10. Fu, L.L.; Wu, G.H.; Zhou, C.; Xiu, Z.Y.; Yang, W.S.; Qiao, J. Effect of Microstructure on the Dimensional Stability of Extruded Pure Aluminum. *Materials* **2021**, *14*, 4797. [CrossRef]
11. Song, Y.F.; Du, W.; Zhao, L.Z.; Zeng, L.J.; Liu, W.H.; Chen, Y.Q.; Zhu, B.W.; Zhang, X.F.; Ding, X.F. The coupling influences and corresponding mechanisms of high efficiency thermal-magnetic treatments on the dimensional stability of Al-Cu-Mg alloy. *J. Alloy. Compd.* **2022**, *928*, 167187. [CrossRef]
12. Song, Y.F.; Ding, X.F.; Xiao, L.R.; Liu, W.H.; Chen, Y.Q.; Zhao, X.J. The Effect of Ni Plating on the Residual Stress and Micro-Yield Strength in an Al-Cu-Mg Alloy Under Different Diffusion Treatments. *JOM-US* **2019**, *71*, 4370–4377. [CrossRef]
13. Qiu, W.T.; Jiang, H.W.; Xiao, Z.; Pang, Y.; Sheng, X.F.; Li, Z. Effect of creep annealing on the dimensional stability of dispersion strengthened copper alloy. *J. Alloy. Compd.* **2021**, *887*, 161321. [CrossRef]
14. Sun, L.; Chen, L.; Guo, Y.Y.; Zhao, G.Q. Experimental Study and Optimization on Solution and Artificial Aging of Cold-Rolled 2024 Al Alloy Sheet. *J. Mater. Eng. Perform.* **2022**, *2022*, 1–13. [CrossRef]
15. Czerwinski, F. Thermal Stability of Aluminum Alloys. *Materials* **2020**, *13*, 3441. [CrossRef]
16. Zhou, L.; Chen, K.H.; Chen, S.Y.; Zhang, X.L.; Fan, S.M.; Huang, L.P. Comparison of hardenability and over-aging precipitation behaviour of three 7xxx aluminium alloys. *Mater. Sci. Technol.* **2019**, *35*, 637–644. [CrossRef]
17. Wen, K.; Xiong, B.Q.; Zhang, Y.A.; Li, X.W.; Li, Z.H.; Yan, L.Z.; Yan, H.W.; Liu, H.W. Aging precipitation characteristics and tensile properties of Al–Zn–Mg–Cu alloys with different additional Zn contents. *Rare Met.* **2021**, *40*, 2160–2166. [CrossRef]
18. Jung, C.Y.; Lee, J.H. Crack closure and flexural tensile capacity with SMA fibers randomlyembedded on tensile side of mortar beams. *Nanotechnol. Rev.* **2020**, *9*, 354–366. [CrossRef]
19. Zaroog, O.S.; Ali, A.; Sahari, B.B.; Zahari, R. Modeling of residual stress relaxation of fatigue in 2024-T351 aluminium alloy. *Int. J. Fatigue* **2011**, *33*, 279–285. [CrossRef]
20. Zheng, J.H.; Lin, J.G.; Lee, J.; Pan, R.; Li, C.; Davies, C.M. A novel constitutive model for multi-step stress relaxation ageing of a pre-strained 7xxx series alloy. *Int. J. Plast.* **2018**, *106*, 31–47. [CrossRef]
21. Petre, M.; Dinu, C.; Drăghici, N.C.; Andrei, V. Prediction of the residual stress after quenching of 6061 aluminium alloy plates by using mathematical modelling. *ITM Web Conf.* **2020**, *34*, 02007. [CrossRef]
22. LI, N.K.; Ling, G.; Nie, B.; Zhou, J.; Li, F.T. *Aluminum Alloy Material and Its Heat Treatment Technology*; Metallurgical Industry Press: Beijing, China, 2012; pp. 270–291.
23. Wang, Z.T. *Heat Treatment Process of Wrought Aluminum Alloy*; Central South University Press: Changsha, China, 2011; pp. 302–313.
24. Kim, W.; Raman, S. On the selection of flatness measurement points in coordinate measuring machine inspection. *Int. J. Mach. Tools Manuf.* **2000**, *40*, 427–443. [CrossRef]
25. He, Z.R.; Shen, Y.Z.; Tao, J.; Chen, H.F.; Zeng, X.F.; Huang, X.; El-Aty, A.A. Laser shock peening regulating aluminum alloy surface residual stresses for enhancing the mechanical properties: Roles of shock number and energy. *Surf. Coat. Technol.* **2021**, *421*, 127481. [CrossRef]
26. Duncheva, G.V.; Maximov, J.T.; Dunchev, V.P.; Anchev, A.P.; Atanasov, T.P.; Capek, J. Single toroidal roller burnishing of 2024-T3 Al alloy implemented as mixed burnishing process. *Int. J. Adv. Manuf. Technol.* **2020**, *111*, 3559–3570. [CrossRef]
27. Lu, L.X.; Sun, J.; Li, L.; Xiong, Q.C. Study on surface characteristics of 7050-T7451 aluminum alloy by ultrasonic surface rolling process. *Int. J. Adv. Manuf. Technol.* **2016**, *87*, 2533–2539. [CrossRef]
28. Zhao, J.G.; Liu, Z.Y.; Bai, S.; Zeng, D.P.; Luo, L.; Wang, J. Effects of natural aging on the formation and strengthening effect of G.P. zones in a retrogression and re-aged Al–Zn–Mg–Cu alloy. *J. Alloy. Compd.* **2020**, *829*, 154469. [CrossRef]
29. Li, S.; Dong, H.G.; Shi, L.; Wang, X.X.; Liu, Z.Y.; Shang Guan, L.J.; Tian, Y.S. The Effects of Heat Straightening Temperature on the Microstructure and Properties of 7N01 Aluminum Alloy. *Materials* **2019**, *12*, 2949. [CrossRef]
30. Liu, J.Z.; Hu, R.; Zheng, J.L.; Zhang, Y.D.; Ding, Z.G.; Liu, W.; Zhu, Y.T.; Sha, G. Formation of solute nanostructures in an Al–Zn–Mg alloy during long-term natural aging. *J. Alloy. Compd.* **2020**, *821*, 153572. [CrossRef]
31. Gai, P.T.; Huang, X.; Zeng, Y.S.; Wang, M.T. Research on Microstructure and Properties of Aged 7050T451 Aluminum Alloy. *Metall. Mater. Trans.* **2014**, *45*, 419–426. [CrossRef]
32. Wolfstieg, U.; Macherauch, E. 1.1 Zur Definition von Eigenspannungen. *HTM J. Heat Treat. Mater.* **1976**, *31*, 2–3. [CrossRef]
33. Rashed, H.M.M.A. *Control of Distortion in Aluminium Heat Treatment. Fundamentals of Aluminium Metallurgy*; Lumley, R.N., Ed.; Woodhead Publishing: Dhaka, Bangladesh, 2018; pp. 495–524.

34. Wei, L.J.; Wang, D.W.; Li, H.S.; Xie, D.; Ye, F.; Song, R.K.; Zheng, G.; Wu, S.J. Effects of Cryogenic Treatment on the Microstructure and Residual Stress of 7075 Aluminum Alloy. *Metals* **2018**, *8*, 273. [CrossRef]
35. Dong, Y.B.; Shao, W.Z.; Jiang, J.T.; Zhang, B.Y.; Zhen, L. Minimization of Residual Stress in an Al-Cu Alloy Forged Plate by Different Heat Treatments. *J. Mater. Eng. Perform.* **2015**, *24*, 2256–2265. [CrossRef]
36. Szpunar, J.A.; Narayanan, R.; Li, H. Computer Model of Recrystallization Texture in Aluminum Alloys. *J. Mater. Eng. Perform.* **2007**, *22*, 928–933. [CrossRef]
37. Chen, J.F.; Jiang, J.T.; Zhen, L.; Shao, W.Z. Stress relaxation behavior of an Al–Zn–Mg–Cu alloy in simulated age-forming process. *J. Mater. Process. Technol.* **2013**, *214*, 775–783. [CrossRef]
38. Sun, Y.S.; Jiang, F.L.; Zhang, H.; Su, J.; Yuan, W.H. Residual stress relief in Al–Zn–Mg–Cu alloy by a new multistage interrupted artificial aging treatment. *Mater. Des.* **2016**, *92*, 281–287. [CrossRef]
39. Cao, Y.F.; Jiang, L.T.; Gong, D.; Chen, G.Q.; Xiu, Z.Y.; Cheng, Y.M.; Wang, X.F.; Wu, G.H. Quantitative study of dimensional stability mechanism and microstructure evolution during precipitation process of 2024Al alloy. *J. Mater. Sci. Technol.* **2021**, *90*, 85–94. [CrossRef]
40. Park, J.K.; Ardell, A.J. Correlation between microstructure and calorimetric behavior of aluminum alloy 7075 and Al-Zn-Mg alloys in various tempers. *Mater. Sci. Eng. A* **1989**, *114*, 197–203. [CrossRef]
41. Soyama, J.; Rios, C.T. Effect of Subcritical Annealing on the Microstructure and Mechanical Properties of a Precipitation-Hardened Al-Zn-Mg-Cu Alloy. *J. Mater. Eng. Perform.* **2021**, *30*, 1012–1021. [CrossRef]
42. Kilic, S.; Kacar, I.; Sahin, M.; Ozturk, F.; Erdem, O. Effects of Aging Temperature, Time, and Pre-Strain on Mechanical Properties of AA7075. *Mater. Res.* **2019**, *22*, 1–13. [CrossRef]
43. Panigrahi, S.K.; Jayaganthan, R. Effect of Annealing on Thermal Stability, Precipitate Evolution, and Mechanical Properties of Cryorolled Al 7075 Alloy. *Metall. Mater. Trans.* **2011**, *42*, 3208–3217. [CrossRef]
44. Tajally, M.; Huda, Z.; Masjuki, H.H. Effect of deformation and recrystallization conditions on tensile behavior of aluminum alloy 7075. *Met. Sci. Heat Treat.* **2011**, *53*, 165–168. [CrossRef]

Disclaimer/Publisher's Note: The statements, opinions and data contained in all publications are solely those of the individual author(s) and contributor(s) and not of MDPI and/or the editor(s). MDPI and/or the editor(s) disclaim responsibility for any injury to people or property resulting from any ideas, methods, instructions or products referred to in the content.